Journal of Computational Physics **178,** 161–174 (2002)
doi:10.1006/jcph.2002.7025, available online at http://www.idealibrary.com on IDEAL®

Lattice Gas Modeling of Scour Formation under Submarine Pipelines

Alexandre Dupuis and Bastien Chopard

CUI—Computer Science Departement, University of Geneva, 24, rue Général-Dufour, CH—1211 Geneva, Switzerland
E-mail: Alexandre.Dupuis@cui.unige.ch and Bastien.Chopard@cui.unige.ch

Received March 19, 2001; revised December 10, 2001

The so-called lattice Boltzmann method is used to implement a numerical model for erosion, transport, and deposition of sediment due to the action of a streaming fluid. This approach is applied to describe the formation of a scour under a submarine pipe. Both static and dynamic properties of the process are well reproduced by our computer simulations. © 2002 Elsevier Science (USA)

Key Words: lattice Boltzmann method; sediment transport; erosion and deposition processes; scour formation phenomena.

1. INTRODUCTION

The lattice Boltzmann or, more generally, lattice gas methods are rather new numerical techniques aimed at modeling a physical system in terms of the dynamics of fictitious particles [9, 25]. This method is now considered a serious alternative to standard computational fluid dynamics [2]. The main idea of this approach is to model the physical reality at a mesoscopic level: the generic features of microscopic processes can be expressed through simple rules, from which the desired macroscopic behavior emerges as a collective effect of the interactions between the many elementary components.

In the past few years, lattice gas models have been extensively used to simulate complex flows [5, 23, 25] (such as flows in complicated geometries and multiphase flows), as well as flows of granular material [15]. This approach has also been successfully applied to snow transport by wind [20, 21].

An interesting advantage of the lattice gas models is their simplicity, first from the numerical point of view (a 3D fluid code amounts to about 100 lines in Fortran) and, second, due to the ease of adding new physical processes in the model. Furthermore their implementation on a parallel computer is straightforward and an object-oriented approach can be efficiently devised [11].

0021-9991/02 $35.00

Lattice gas models can typically be applied to describe sediment transport and erosion appearing around submarine pipelines. Such pipelines are commonly used to transport oil, gas, or even water on the sea bed. At installation time, they rest on an erodible bed. The current around the pipe causes the formation of an excavation below the pipe, called a scour. The scour can typically reach a depth approximately equal to the pipe diameter. At first sight, these scours might damage the pipe due to vibration effects which are due to the current underneath the pipe. However considering that an important part of the installation cost is devoted to the pipe protection from environmental changes, current, or even anchoring, these scours can be seen as an opportunity to self-bury the pipe. A prediction of their formation and consequently a better understanding of the whole phenomena becomes necessary.

In this contribution, we show that the lattice gas approach can successfully address the problem of the scour formation under a submarine pipeline in a steady current.

The scour formation process has been studied in flumes by various authors [6, 16, 19]. Numerical models have been proposed in [3, 17, 22]. They are based on an iterative process which consists of computing the velocity repartition using a finite-difference scheme and then in determining the change of the bed.

The numerical approach we propose here to describe scour formation is radically different from standard CFD techniques since it uses a particle-based approach. Computer simulations of our lattice gas model are in good agreement with the observations found in the literature concerning the scour profile, the depth below the pipe, and the velocity distribution along the system.

The paper is organized as follows. In Section 2, the numerical model is explained. In Section 3, the main phenomenology of the scour formation process is recalled. Section 4 presents the results of the simulations and Section 5 draws some conclusions.

2. THE MODEL

2.1. Overview

In this section we explain the salient features of our model. We consider a mixed lattice Boltzmann (LB) and cellular automata (CA) approach (see, for instance, [4, 9, 25] for a general description of the method).

The fluid-particle system is described in terms of a mesoscopic dynamics: fictitious fluid and sediment particles move on a regular lattice synchronously at discrete time steps. An interaction is defined between the particles that meet simultaneously at the same lattice site. Fluid particles obey collision rules which reproduce, in the macroscopic limit, the Navier–Stokes equation. The granular material moves under the combined effect of the local fluid velocity field and gravity.

As they reach the ground, the solid particles pile up and topple if necessary, changing in this way the boundary conditions for the fluid. The fluid particles bounce back on the deposited granular material. At the top of the deposition layer, erosion takes place, and if the fluid flows fast enough, it can pick up solid particles and transport them further away.

As we see, our model contains several adjustable parameters. Some of them are standard parameters, such as, for instance, the falling speed of the granular material or the repose angle of the sediments. Other parameters, like our probablity of erosion, are specific to our model and some extra work may be needed to relate them to the usual quantities introduced

in the traditional approach. For instance, the grain size does not enter explicitly in our model. However, our parameters should be considered as some function of the grain size, and although we do not attempt to express this dependence here, a calibration could be done. Our main goal is to show that the LB approach is suitable to address time-dependent erosion processes and we demonstrate it by analyzing the scour formation for a particular set of parameters that we believe to be repesentative of the generic case.

2.2. The Fluid Model

The fluid is represented by a LB model, that is by density distribution functions $f_i(\mathbf{r}, t)$ giving the probability that a fictitious fluid particle with velocity $\mathbf{v}_i$ enters the lattice site $\mathbf{r}$ at discrete time t. The admissible velocities $\mathbf{v}_i$ are dependent on the lattice topology. Usually, i runs between 0 and z, where z is the lattice coordination number (i.e., the number of lattice links). By convention $\mathbf{v}_0 = 0$ and f_0 represents the density distribution of particles at rest. For many lattice topologies the set of vectors $\mathbf{v}_i$ can be divided into slow and fast velocities: slow velocities correspond to a jump to a nearest neighbor site while fast velocities imply a jump to a second nearest neighbor.

The dynamics we consider for f_i is given by the so-called BGK model [4, 8, 9, 25],

$$f_i(\mathbf{r} + \tau\mathbf{v}_i, t + \tau) = \omega f_i^{(0)}(\mathbf{r}, t) + (1 - \omega) f_i(\mathbf{r}, t), \tag{1}$$

where τ is the time step of the simulation, $1/\omega$ the relaxation time, and $f_i^{(0)}$ the local equilibrium, which is a function of the density $\rho = \sum_{i=0}^{z} m_i f_i$ and the fluid velocity $\mathbf{u}$ defined through the relation $\rho\mathbf{u} = \sum_{i=0}^{z} m_i f_i \mathbf{v}_i$. The quantities m_i are weights associated with the lattice directions, and $m_0 = 1$ by definition.

It can be shown (see, for instance, [8, 9, 25]) that Eq. (1) reproduces a hydrodynamical behavior if the local equilibrium functions are chosen as follows (Greek indices label the spatial coordinates):

$$f_i^{(0)} = \rho\left[\frac{1}{C_2}\frac{c_s^2}{v^2} + \frac{1}{C_2}\frac{\mathbf{v}_i \cdot \mathbf{u}}{v^2} + \frac{1}{2C_4 v^4}\sum_{\alpha\beta}\left(v_{i\alpha}v_{i\beta} - v^2\frac{C_4}{C_2}\delta_{\alpha\beta}\right)u_\alpha u_\beta\right],$$

$$f_0^{(0)} = \rho\left[1 - \frac{C_0}{C_2}\frac{c_s^2}{v^2} + \left(\frac{C_0}{2C_2} - \frac{C_2}{2C_4}\right)\frac{u^2}{v^2}\right].$$

Table I gives the values of the coefficients C_k and the weight m_i for a few standard lattice topologies noted DdQ$(z + 1)$, where d is the spatial dimension. The quantity v gives the speed unit. It corresponds to the modulus of the slow velocities. Note that the expression we propose here for the local equilibrium distribution is exactly equivalent to the standard one (see [25]). However, the formulation in terms of the topological coefficients C_0, C_2, and C_4 and weights m_i is less common in the framework of hydrodynamics. It is however quite convenient when considering other physical systems [8], such as wave propagation or diffusion processes, because it clearly decouples the contribution due to the topologies from the contribution due to the physics.

As mentioned earlier, Eq. (1) with (1) for the local equilibrium distributions is equivalent to the continuity equation and Navier–Stokes equation with speed of sound c_s and viscosity

$$\nu = \tau v^2 \frac{C_4}{C_2}\left(\frac{1}{\omega} - \frac{1}{2}\right). \tag{2}$$

TABLE I
The Geometrical Coefficients Necessary to Compute the Local Equilibrium Distributions in a LB Simulation

Model	Slow velocities	Fast velocities	C_0	C_2	C_4
D1Q3	$\|v_i\| = v, m_i = 1$		2	2	2/3
D2Q9	$\|v_i\| = v, m_i = 4$	$\|v_i\| = \sqrt{2}v, m_i = 1$	20	12	4
D2Q7	$\|v_i\| = v, m_i = 1$		6	3	3/4
D3Q15	$\|v_i\| = v, m_i = 1$	$\|v_i\| = \sqrt{3}v, m_i = 1/8$	7	3	1
D3Q19	$\|v_i\| = v, m_i = 2$	$\|v_i\| = \sqrt{2}v, m_i = 1$	24	12	4

Note. The quantity v is the ratio of the lattice spacing to the time step τ and $m_0 = 1$ for all models.

Thus, this approach has two free parameters, c_s and ω. An obvious constraint on these parameters is that f_i and the viscosity remain positive, which implies that $\omega < 2$ and $c_s^2 < (C_2/C_0)v^2$. A commonly chosen value for c_s is $c_s^2 = v^2(C_4/C_2)$, which improves the numerical stability.

The LB fluid model has been extensively validated in the literature [2, 5, 25] and is known to reproduce correctly the time-dependent Navier–Stokes equation. An important class of applications in hydrodynamics is high Reynolds number flows. A simple way to reach high Reynolds numbers is to reduce the viscosity by making ω close to 2. Unfortunately, numerical instabilities may develop in this case, due to velocity gradients. To alleviate this problem, one can have recourse to the so-called Smagorinsky subgrid model. This is standard approach in computational fluid dynamics and was first proposed for LBGK models by Hou *et al*. [13]. One assumes that a turbulent viscosity (ν_t) results from the unresolved scales, that is, the scales below the lattice spacing λ. These scales are thus filtered. The main idea is to increase locally the relaxation time $1/\omega$ by defining a space and time variable relaxation time $1/\omega_{tot}$.

Then the total viscosity is split as

$$\nu_{tot} = \nu + \nu_t,$$

where ν is the original viscosity given by Eq. (2) with the original relaxation time $1/\omega$. The new contribution ν_t is the so-called turbulent viscosity resulting from the filtered scales. In the Smagorinsky model [24], it is expressed as

$$\nu_t = (C_{\text{smago}}\Delta)^2|S|, \tag{3}$$

where Δ is the filter size, whose magnitude usually corresponds to the grid spacing, and $|S| = \sqrt{2S_{\alpha\beta}S_{\alpha\beta}}$ is the magnitude of the strain-rate tensor $S_{\alpha\beta} = 1/2(\partial_\beta u_\alpha + \partial_\alpha u_\beta)$. Thus, the larger the $|S|$, the larger the turbulent viscosity, so that the total viscosity is more important in regions close to obstacles.

In the LB scheme, the quantity $S_{\alpha\beta}$ can be computed locally, without taking extra derivatives, by only considering the nonequilibrium momentum tensor as [8]

$$S_{\alpha\beta} = -\frac{\omega_{tot}}{2\rho\tau}\frac{C_2}{C_4}\Pi^{(1)}_{\alpha\beta} = -\frac{\omega_{tot}}{2\rho\tau}\frac{C_2}{C_4}\sum_i m_i v_{i\alpha} v_{i\beta}\left(f_i - f_i^{(0)}\right). \tag{4}$$

Thus, from (3) and (4), the turbulent viscosity can be expressed as

$$\nu_t = \frac{\omega_{tot}}{\sqrt{2}\rho\tau}\frac{C_2}{C_4}(C_{\text{smago}}\Delta)^2\sqrt{Q^2}, \tag{5}$$

where $Q^2 = \Pi^{(1)}_{\alpha\beta}\Pi^{(1)}_{\alpha\beta}$. From Eq. (2), one has

$$\frac{1}{\omega_{tot}} = \frac{\tau}{\lambda^2}\frac{C_2}{C_4}(\nu + \nu_t) + \frac{1}{2}. \tag{6}$$

Considering that also

$$\frac{\tau}{\lambda^2}\frac{C_2}{C_4}\nu + \frac{1}{2} = \frac{1}{\omega}$$

and substituting Eq. (5) into Eq. (6), one can solve the resulting second-order equation and then express the local relaxation time as

$$\frac{1}{\omega_{tot}} = \frac{1}{2}\left(\sqrt{\frac{1}{\omega^2} + \frac{1}{\lambda^2}(C_{\text{smago}}\Delta)^2\left(\frac{C_2}{C_4}\right)^2\frac{\sqrt{8Q^2}}{\rho}} + \frac{1}{\omega}\right). \tag{7}$$

The quantity C_{smago} (typically smaller than 0.5) tunes the effect of the subgrid model and should be adjusted empirically depending on the desired flow pattern.

The problem of ajusting correctly C_{smago} remains open. In order to model the boundary layer near a wall, one may expect that the value of C_{smago} is zero at the boundary of an obstacle and then increases to reach its bulk value as one gets away from the wall. No obvious theory describes how this variation should be and the simulation we performed did not show a real change in the main features of the flow when C_{smago} is varied. Therefore, we assume that the simplified procedure of having a constant nonzero is enough in the present case.

As an illustration, we present in Fig. 1 the velocity pattern we obtain within this framework in the case of the flow around a pipeline sitting on a flat surface.

The flow we consider is turbulent (Re = 7000), and for this reason, we plot the stationary average streamlines and average horizontal velocity profile. This simulation compares well

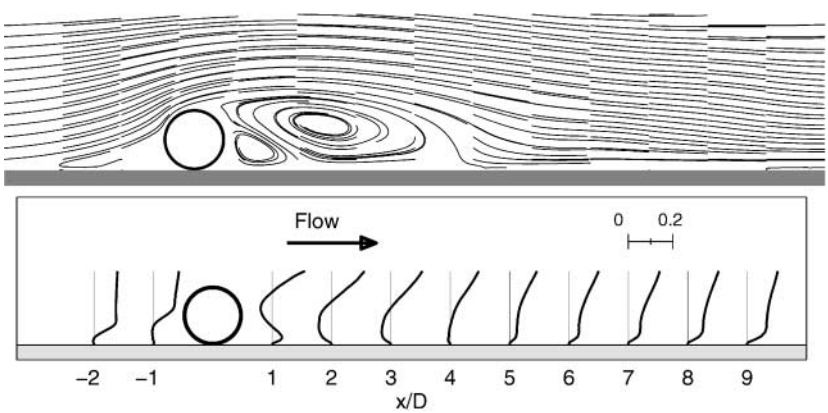

FIG. 1. Average flow pattern around a pipe in a turbulent regime, as obtained with the LB method. The Reynolds number is Re = 7000, obtained with $1/\omega = 0.5023$, $(C_{\text{smago}}\Delta)^2 = 0.4\lambda^2$. The entry speed is $u_{\text{entry}} = 0.1\lambda/\tau$ and the cylinder diameter $D = 20\lambda$. The upper panel shows the streamlines and the lower one the horizontal velocity profile at several locations. Distances are given in pipe diameters and velocities in lattice units.

with the experiment by Jensen [14]. In addition, this flow is generic (with respect to the size of the main eddies and reattachement points) of the situations considered in laboratory experiments when studying the scour formation process [3, 16].

2.3. The Sediment Model

After the fluid motion, the second important ingredient of our model is the sediment. Here, particles are represented by an integer $n(\mathbf{r}, t) \geq 0$, indicating how many pseudoparticles are present at site $\mathbf{r}$ and time t. Sediments move on the same lattice as the fluid particles and interact with them. Since $n(\mathbf{r}, t)$ can take any positive value, we term our model a multiparticle CA.

It is important to remember that in our mesoscopic approach, we do not try to represent a specific granular material. Rather, we want to capture the generic features of the erosion–deposition process. The existence of universal behaviors in systems with many interacting particles is common in many areas of science and there are numerous examples where the macroscopic behavior depends very little on the microscopic details of the system. For this reason, we may expect (and this is confirmed by our results) that, at first approximation, our dynamics of fictitious particle produces the same deposition patterns as real systems, even if all parameters are not of the correct order of magnitude.

2.3.1. *Transport Rule*

In this section, we describe the rule of motion for the sediment particles. After each time step, the particles jump to a nearest-neighbor site, under the action of the local fluid flow and gravity force. Gravity is taken into account by imposing a falling speed $\mathbf{u}_{\text{fall}}$ to the particles. In the simplest version of our model, the suspensions are passive particles and their presence does not modify the flow field, except when they form a solid deposit (i.e., a new boundary condition). However, it would be quite easy to modify the fluid properties so as to make the inverse relaxation time ω vary according to the local density of transported particles to account for the fact that the fluid viscosity depends on the concentration of the suspensions.

If the local fluid velocity at site $\mathbf{r}$ is $\mathbf{u}(\mathbf{r}, t)$, the particles located at that site will move to site $\mathbf{r} + \tau_s(\mathbf{u} + \mathbf{u}_{\text{fall}})$, where τ_s is the time unit associated with the motion of the granular particles. Unfortunately, this new location is usually not a lattice site. The solution to this problem is then to consider a stochastic motion: each of the $n(\mathbf{r}, t)$ particles jumps to a neighboring site $\mathbf{r} + \tau\mathbf{v}_i$ with a probability p_i proportional to the projection of $\tau_s(\mathbf{u} + \mathbf{u}_{\text{fall}})$ on the lattice direction $\tau\mathbf{v}_i$. The quantity τ_s is adjusted so as to maximize the probability of motion, while ensuring that the jumps are always smaller than a lattice constant. An example of the transport rule is presented in Fig. 2 for the hexagonal D2Q7 model (the other topologies are widely treated in [21]). In this case (see Fig. 2), three probabilities p_0, p_{i_1}, and p_{i_2} must be computed using the two relations

$$\frac{\sin\alpha}{\tau_s|\mathbf{u} + \mathbf{u}_{\text{fall}}|} = \frac{\sin\beta}{p_{i_2}} = \frac{\sin\gamma}{p_{i_1}}, \quad p_0 + p_{i_1} + p_{i_2} = 1,$$

where α equals 60 degrees.

This stochastic cellular automata rule produces a particle motion with the correct average trajectory and a variance which can be interpreted as a local diffusive behavior [21]. Indeed,

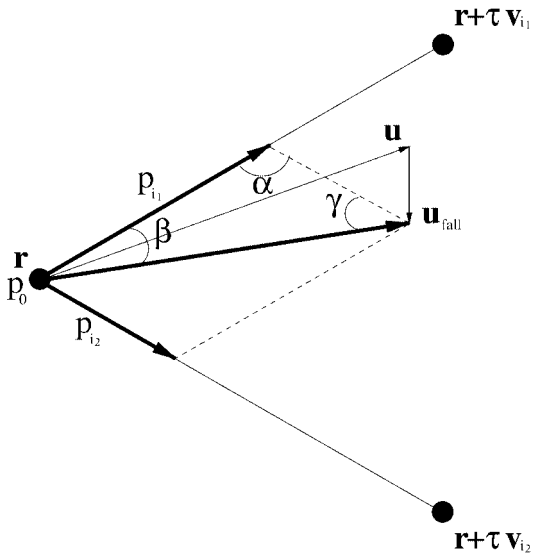

FIG. 2. Illustration of the motion rule in case of the D2Q7 model. Shown are three lattice sites, $\mathbf{r}$, $\mathbf{r} + \tau \mathbf{v}_{i_1}$, and $\mathbf{r} + \tau \mathbf{v}_{i_2}$, which correspond to the possible destinations of the particle subject to a fluid drag $\mathbf{u}$ and a fall velocity $\mathbf{u}_{\text{fall}}$. The corresponding probabilities p_{i_1} and p_{i_2} are obtained by the projection shown in the figure.

it can be shown [21] that the diffusion coefficient can be expressed as $D = D^*(\lambda^2/\tau)$, where λ and τ are the space and time spacings, respectively. The quantity D^* is a dimensionless coefficient related to the lattice topology, which in our case is $D^* \approx 1/2$. Therefore, when reducing the lattice spacing with the usual constraint $\lambda = \tau$, the full diffusion constant decreases as $O(\lambda)$ and vanishes for fine-enough grids. However, we noticed from various numerical simulations that the deposition patterns we obtain are quite robust to a change of the grid size. The noise produced by our transport rule seems necessary to initiate erosion (e.g., ripple formations) but the amplitude of this noise is much less relevant.

Note that in this model there is no need to describe transport mechanisms other than the one defined above: creeping, saltation, and suspension all naturally emerge from our rule at the macroscopic scale [21].

2.3.2. *Deposition Rule*

The next aspect of the particle dynamics is the deposition rule. Under the combined effect of the fluid and gravity, particles can land on a solid site (e.g., the bottom of the system or the top of the deposition layer). Motion is no longer possible and particles start piling up. In our model, up to N_{thres} particles can accumulate on a given site (N_{thres} gives a way to specify the spatial scale of the granular particles with respect to the fluid system). When this limit is reached, the site solidifies and new incoming particles pile up on the site directly above. The solid sites formed in this way represent obstacles on which the fluid particles bounce back from where they came. Thus, this solidification process implies a dynamically changing boundary condition for the fluid.

Note that, on the other hand, the fluid is not affected by the presence of the rest particles piling up on top of a solid site. Also, these rest particles are no longer subject to the suspension transport rule. Only the erosion mechanism discussed below can move them away.

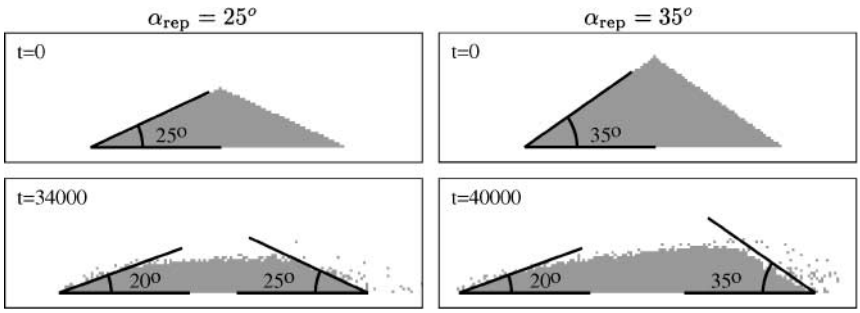

FIG. 3. Evolution of stable piles subject to a flow streaming from left to right, as produced by our transport, deposition, and erosion rules. Two different angles of repose α_{rep} are considered. The variable t indicates the number of iterations. At $t = 0$, the flow is applied and a stationary regime is reached after a few thousand iterations. Note that the effect of the flow is to modify the leeward slopes and also to make piles move to the right.

As sediment particles do not have infinite cohesion, it is realistic to consider the following toppling rule: when a lattice site contains an excess of δN deposited particles with respect to its left or right neighbors (in 2D), toppling occurs. During this process, all unstable sites send a given portion of their grains in excess to the less-occupied neighbors. With this rule, the stable configuration may not be reached in one iteration, and for this reason, the model allows the toppling and transport processes to take place at different time scales.

The quantities δN and N_{thres} give a simple way to adjust the angle of repose of the pile. In the stable state, the model tolerates a maximum difference of δN particles between two adjacent sites. Two solidified sites are at least horizontally separated by k sites, where $k = [N_{\text{thres}}/\delta N]$. Hence, the angle of repose α_{rep} satisfies

$$\tan \alpha_{\text{rep}} = 1/k.$$

Figure 3 illustrates the effect of changing α_{rep} on two toppling simulations. At the initial stage ($t = 0$) one considers two piles prepared with their angle of repose (in this example, 25° and 35°, respectively). Then a flow from left to right is turned on and the piles have to adjust by taking into account the erosion (whose mechanism is explained below) produced by the flow. One observes that the downstream slopes keep the same angle while the upstream slopes become less steep.

2.3.3. *Erosion*

Finally, we describe the rule implementing the erosion process. The mechanism we propose is quite simple and corresponds to making again the deposited grains available for transport: with probability p_{erosion} each particle belonging to the first N_{thres} particles of the deposition layer (either a solid site or the rest particles that have accumulated directly above) is moved one lattice spacing up, into a site where the transport rule apply.

If the local fluid velocity on that site is big enough, the particle will be picked up and moved further away. Otherwise, if the flow is slow, the resulting motion will be to land again on the same site where the particle started off.

This rule captures the important effect that a strong flow will result in an important erosion process. It also implements naturally the idea that erosion starts only if the local speed is larger than some threshold. One could also make the probability parameter p_{erosion} depend on

the amount of particles already in suspension, as it is often suggested in phenomenological models. However, in our simulations this does not turn out to be necessary and p_{erosion} is a constant that is modified only from one simulation to the other, when representing different qualities of sediment.

2.4. Note on the Model Parameters

Several parameters can be tuned to modify the behavior of our model. For the fluid, one can typically vary the entry speed (u_{entry}) and change the viscosity (by changing ω).

The interaction between the fluid and the suspensions is determined by the falling speed u_{fall}. This parameter accounts for the ratio of the fluid and solid densities and the grain diameter in a way that we do not make explicit her. Similarly, the erosion probablity p_{erosion} is a quantity containing the effect of several parameters, such as the lift force, grain mobility, and interparticle cohesion.

The properties of the sediments are described by the angle of repose α_{rep} and the quantity N_{thres}, which, as explained previously, is the amount of grain that is needed to fill a region whose height and width is one lattice spacing (in 2D).

Thus, as opposed to the conventional description, the grain diameter is not an independent parameter of our model. However, its effect on u_{fall}, p_{erosion}, N_{thres} could be worked out. Such a calibration is not the purpose of this paper and we leave the detailed analysis of the dependence of our model upon its parameter for a future investigation. The rest of this study focuses on the capability of our approach to simulate the scour formation under a submarine pipe and, to this end, we restrict ourselves to a set of parameters which reproduces the generic features of the process. These values could be used as guidelines for other simulations.

3. SCOUR FORMATION PROCESS

This section reviews some phenomenological features of the scour formation process under a pipe [12, 27]. Figure 4 presents the situation of interest. The scour which forms

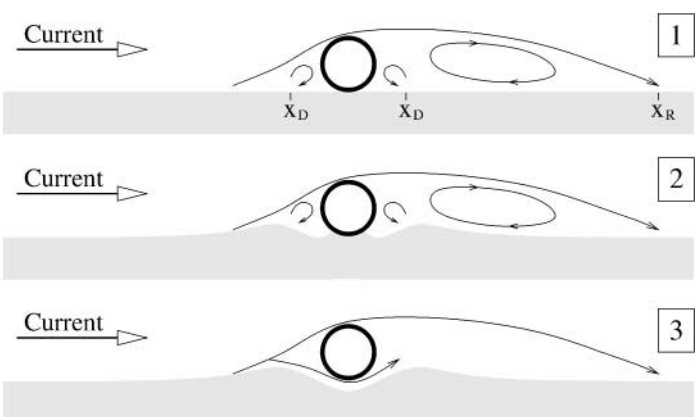

FIG. 4. Three main stages of the scour onset process under a unidirectional current. (1) Due to the current, three main vortices appear in the pipe neighborhood. (2) The two small vortices up- and downstream of the pipe start to dig a hole. (3) After a while, the holes meet each other below the pipe and the scour formation process breaks out. x_D and x_R denote reattachment points.

under the pipe occurs in two main phases, namely the onset and the erosion. The onset of the scour is directly related to the two vortices in front of and behind the pipe. Each one digs up a hole. The scour formation process breaks out when these holes meet together under the pipe. The onset process is illustrated in Fig. 4.

When the water has started to flow underneath the pipe, the scour formation stage takes place. First, the gap under the pipe is small while the downstream hill is relatively high. At this point, the pressure upstream of the pipe is rather high and consequently the fluid is accelerated. Many sediment particles are ejected and the scour development is fast. Then, as the scour depth increases, the velocity under the pipe decreases. It follows that the scour development slows down and progressively reaches an equilibrium.

Various laboratory experiments (see, for example, [16]) show that the depth of the scour depends essentially on the pipe diameter D, the flow velocity V, the kinematic viscosity of the fluid, and the sediment properties. These studies also highlight that the ratio between the scour depth and the pipe diameter should be comprised between 0.2 and 1.0.

Also, it turns out that the scour formation process is not too much influenced, in an appropriate range, by turbulence. Indeed for Reynolds numbers between 1×10^4 and 2×10^5, Kjeldsen *et al.* [16], as well as Bijker and Leeuwenstein [1], propose formulae indicating that the scour depth is strongly controlled by the pipe diameter. Following the same idea, Sumer and Fredsøe [26] propose an empirical formula $S/D = 0.6 \pm 0.1$ indicating the dominant role of the pipe diameter.

4. RESULTS

In this section, we present the predictions of our model for the scour formation process in a steady current. We consider a virtual river made up of a layer of fluid on top of an initially flat bed of sediments with uniform properties. A pipeline is laid on the top of the bed, as illustrated in Fig. 5.

Due to the geometry of the problem, a two-dimensional simulation is considered. The x-axis corresponds to the direction perpendicular to the pipe and the z-axis to the vertical direction. The system size is $L_x = 1100$ and $L_z = 70$, in lattice units. The bottom line ($z = 0$) is an impermeable wall on which sand grains are deposited and fluid particles bounce back if they ever reach this region. For the other boundaries of the system, the conditions change depending on whether one considers a fluid or a sand particle.

For the fluid, the system is periodic along the x-axis. All fluid particles that reach the $x = L_x$ line are re-injected on the left side and vice versa. On the line $x = 0$, the fluid is accelerated uniformly so as to produce a water current flowing from left to right, with entry speed $u_{\text{entry}} = 0.1$ (in lattice units). The viscosity is tuned so as to obtain a Reynolds number $\text{Re} \approx 2 \times 10^4$, which is a typical value in scouring experiments [3, 16]. On the upper line ($z = L_z$) a zero vertical velocity is imposed. Note that these boundary

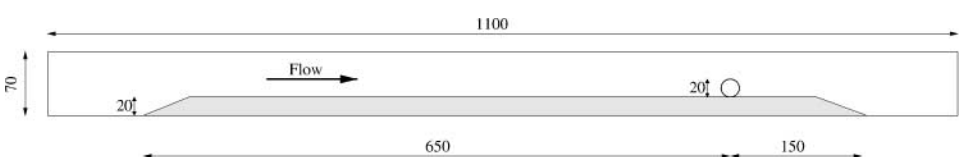

FIG. 5. Geometry of the numerical experiment. Distances are expressed in lattice sites.

TABLE II
Values of the Model Parameters for the Sediments

u_{fall}	N_{thres}	p_{erosion}	α_{rep}
0.006	10	0.01	20°–40°

conditions are implemented so that the total amount of fluid in the simulation remains constant.

For the sediments, the parameters we have chosen for the simulation are summarized in Table II. The falling speed is given in lattice units and the other parameters are pure numbers. The values of these parameters are chosen empirically, so as to reproduce the experiments presented by Mao [18]. However, other values can be considered and other erosion patterns could emerge.

As shown in Fig. 5, the setting of our numerical simulation corresponds precisely to the experiment done by Mao [18]. The simulation starts with an erodible bed and all grains that reach the right (and possibly the top) of the system are lost.

Since the toppling and transport processes are not taking place at the same time scale, we empirically choose to make 20 steps of pure toppling every 20 iterations of the dynamics.

The evolution of the bed profile predicted by our model is shown in Fig. 6, at four typical stages of the scour formation. The profile at $t = 200{,}000$ corresponds to a steady state. It compares well with the experimental profiles found by Mao [18] (white and black circles in the figure). Also, we observe the asymmetry of the scour, which, as expected, is steeper on the left part than on the right part. This gives a good validation of the stationary properties of our model.

Note that the precise value of the repose angle α_{rep} is not critical as long as it is larger than the slopes of the eroded bed (i.e., 14° and 19°). It is admitted that $\alpha_{\text{rep}} = 20°$ is too small to described the sediment properties in Mao's experiment, but we have observed that a larger value of α_{rep} gives the same erosion pattern, too. This is not surprising since the erosion slopes result from the effect of the current and not from the repose angle.

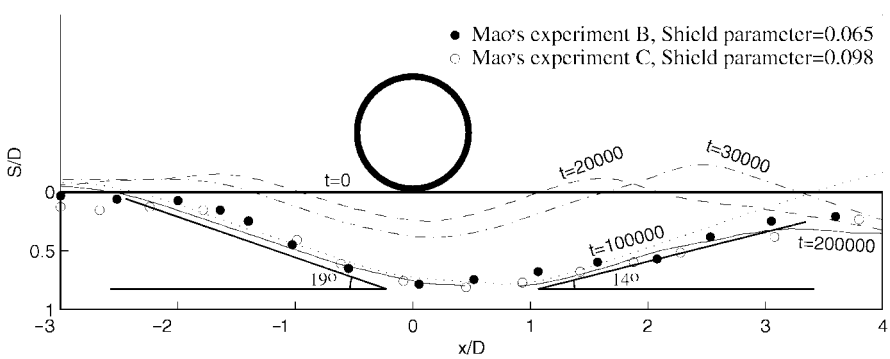

FIG. 6. Characteristic stages of the scour evolution process where S denotes the scour depth, D the pipe diameter, and x the horizontal distance from the center of the pipe. Each iteration is one unit of time. The erosion profile we obtain is in good agreement with the experimental findings shown as the black and white circles.

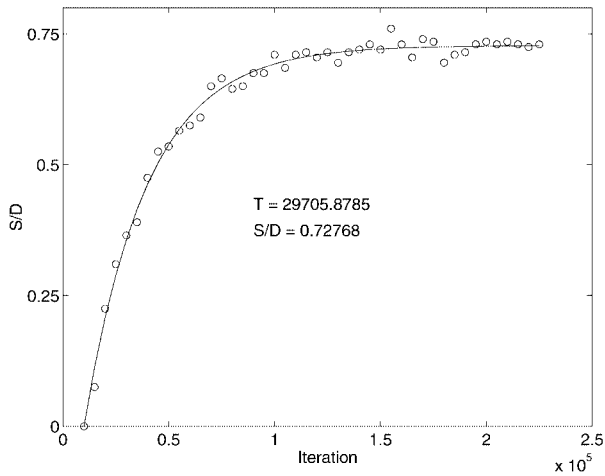

FIG. 7. Time evolution of the scour depth. Simulated depths are displayed as circles, while the solid line is the best fit to Eq. (8). The offset at $S_t = 0$ indicates that the origin of time does not correspond to the beginning of the erosion process.

Our model also gives a dynamical description of the scour formation (Fig. 6 shows the erosion profile at several time steps). In particular, we can observe the protuberance which forms past the pipe and travels downstream, as in real experiments.

In order to have a quantitative validation of the time development, we compare the scour depth we obtain as a function of time with our simulation with the phenomenological relation proposed by Sumer and Fredsøe [26],

$$S_t = S\left(1 - e^{-t/T}\right), \tag{8}$$

describing how the final profile is reached.

In relation (8), S_t denotes the scour depth at time t and S the final equilibrium value. T is the characteristic time scale of the scour process and represents the time period during which a substantial scour develops.

In our simulation we have recorded the scour depth for several time steps. Results are shown in Fig. 7 as white circles. An exponential fit (solid line) shows a very good agreement with the behavior described by (8), thus indicating that the dynamic properties are correctly captured by our approach. Here we obtain a characteristic time $T \approx 29{,}700$ iterations. This quantity depends on the values chosen for the parameters such as u_{fall}, N_{thres}, p_{erosion}. If one modifies them in such a way as to model a larger grain diameter d, one also measures an increase in T. This behavior is in agreement with phenomenological observations [27].

Finally, let us consider the case of a pipe with a spoiler. As mentioned in the introduction, a submarine pipeline is more protected against possible damage when it is buried in the sea bed. The hole resulting from the scour process can be used to self-bury the pipe. Following this idea, spoilers of various angles can be attached to the pipe in order to speed up and increase the scour formation process [7]. Simulations with our method show good results when spoilers are attached to a regular pipe, as shown in Fig. 8, where the effect of the scour depth versus the spoiler angle is compared with experimental observation (see [10] for a more detailed description).

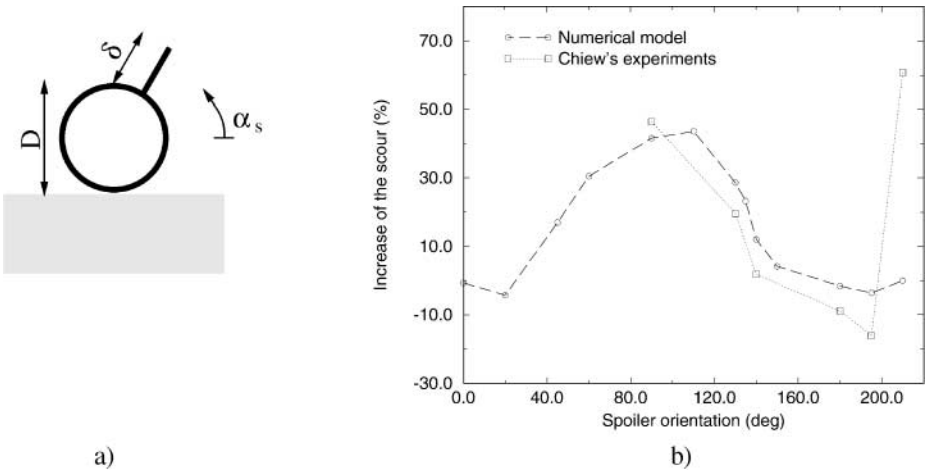

FIG. 8. (a) Submarine pipeline with a spoiler. The spoiler angle is denoted by α_s, the pipe diameter is D, and the spoiler length is δ. (b) Increase in the scour depth versus the spoiler angle α_s. Results from our numerical model are drawn as circles and experiments of Chiew [7] as squares.

5. CONCLUSION

We have presented a lattice gas model incorporating two ingredients, namely water and sediment, in order to simulate the scour formation process around a pipeline subject to a steady current. The shape of the bed at various stages of the simulation reproduces rather accurately the description given in the literature. The fluid properties are also in agreement with experimental or other numerical studies.

Our main result is that erosion phenomena in water currents can be described as a whole with a lattice gas approach. Intuitive mechanisms are implemented to model the various processes at a mesoscopic scale and the method provides a natural flexibility to describe fluid and sediments within the same numerical framework. Another important feature of our approach is the simplicity of the numerical scheme and the ease of parallelizing it. For instance, a typical simulation, involving 200,000 iterations and 80,000 lattice sites, takes about 100 min on a 32-node cluster (Pentium III, 500 MHz).

Notice that here we only focused on the simulation of a steady current. However, it is quite obvious that one should take wave current into account by changing the way the fluid is accelerated in the simulation, without altering the model itself. Also, some extensions to the model are possible, such as considering two classes of sediments, each with its own set of parameters, so as to model grains of different diameters.

ACKNOWLEDGMENTS

This research was funded by the Swiss National Science Foundation. We thank Stefano Ruffo and his group for pointing out to us the problem discussed in this paper, Paul Albuquerque for helpful discussions and appropriate advice, and Stefan Marconi for his corrections.

REFERENCES

1. E. W. Bijker and W. Leeuwenstein. Interaction between pipelines and the sea bed under the influence of waves and currents, in *Sea Bed Mechanics, IUTAM-IUGG Symp,* edited by B. Denness (Graham and Trotman, London, 1984), p. 235.

2. B. Boghosian, *et al*., Eds., *The 7th International Conference on the Discrete Simulation of Fluid Dynamics* (World Scientific, Oxford, 1998).
3. B. Brørs, Numerical modeling of flow and scour at pipelines, *J. Hydraul. Eng*. **125**(5), 511 (1999).
4. S. Chen and G. D. Doolen, Lattice Boltzmann methods for fluid flows, *Annu. Rev. Fluid Mech*. **30**, 329 (1998).
5. Yu Chen, *et al*., Eds., *The 9th International Conference on the Discrete Simulation of Fluid Dynamics, Tokyo, 1999*, Vol. 129, pp. 167–176 (Computer Physics Communications, 2000).
6. Y. M. Chiew, Mechanics of local scour around submarine pipelines, *J. Hydraul. Eng*. **116**(4), 515 (1990).
7. Y. M. Chiew, Effect of spoilers on scour at submarine pipelines, *J. Hydraul. Eng*. **118**(9), 1311 (1992).
8. B. Chopard, P. Luthi, and A. Masselot, *Cellular Automata and Lattice Boltzmann Techniques: An Approach to Model and Simulate Complex Systems, 1998*, available at http:// cui.unige.ch/∼chopard/CA/Book/related.html.
9. B. Chopard and M. Droz, *Cellular Automata Modeling of Physical Systems* (Cambridge University Press, Cambridge, UK, 1998).
10. A. Dupuis and B. Chopard, Lattice gas simulation of sediment flow under submarine pipelines with spoilers, in *Electronic Proceedings of the 4th International Conference on HydroInformatics, Cedars Rapids, USA, July 2000*.
11. A. Dupuis and B. Chopard, An object oriented approach to lattice gas modeling, *Future Generation Comput. Syst*. **16**(5), 523 (2000).
12. G. J. C. M. Hoffmans and H. J. Verheij, *Scour Manual* (Balkema, Rotterdam, 1997).
13. S. Hou, J. Sterling, S. Chen, and G. D. Doolen, A lattice subgrid model for high Reynolds number flows, *Fields Inst. Commun*. **6**, 151 (1996).
14. B. L. Jensen, Large-scale vortices in the wake of a cylinder placed near a wall, in *Second International Conference on Laser Anemometry—Advances ans applications* (Strathclyde, UK, 1987), p. 153.
15. A. Károlyi and J. Kertész, Hydrodynamics cellular automata for granular media, in *Proceedings of the 6th Joint EPS-APS International Conference on Physics Computing: PC '94*, edited by R. Gruber and M. Tomassini (Euro. Phys. Soc., Geneva, Switzerland, 1994), p. 675.
16. S. P. Kjeldsen, O. Gjørsvik, K. G. Bringaker, and J. Jacobsen, Local scour near offshore pipelines, in *Second International Conference on Port and Ocean Engineering under Arctic Conditions* (University of Iceland, 1973), p. 308.
17. F. Li and L. Cheng, Numerical model for local scour under offshore pipelines, *J. Hydraul. Eng*. **125**(4), 400 (1999).
18. Y. Mao, *The Interaction Between a Pipeline and an Erodible Bed*, Technical report (Institute of Hydrodynamics and Hydraulic Engineering, Technical University of Denmark, 1986).
19. Y. Mao, Seabed scour under pipelines, in *Seventh International Conference on Offshore Mechanics and Arctic Engineering* (Houston, TX, 1988), p. 33.
20. A. Masselot and B. Chopard, A lattice Boltzmann model for particle transport and deposition, *Europhys. Lett*. **42**, 259 (1998).
21. A. Masselot, *A new numerical approach to snow transport and deposition by wind: a parallel lattice gas model*, Ph.D. thesis (University of Geneva, 2000), available at http://cui.unige.ch/spc/phds/lbmsnow.pdf.
22. N. Olsen and M. Melaaen, Three-dimensional calculation of scour around cylinders, *J. Hydraul. Eng*. **119**(9), 1048 (1991).
23. D. Rothman and S. Zaleski, *Lattice-Gas Cellular Automata: Simple Models of Complex Hydrodynamics*, Collection Aléa. (Cambridge University Press, Cambridge, UK, 1997).
24. J. Smagorinsky, General circulation experiments with the primitive equations: I. The basic equations, *Mon. Weather Rev*. **91**, 99 (1963).
25. S. Succi, *The Lattice Boltzmann Equation, For Fluid Dynamics and Beyond* (Oxford University Press, Oxford, UK, 2001).
26. B. M. Sumer and J. Fredsøe, A review of wave/current induced scour around pipelines, in *23rd International Coastal Engineering Conference*, Venice, Italy, 1992, Vol. 3, p. 2839.
27. R. Whitehouse, *Scour at Marine Structures* (Telford, London, 1998).